ULTIMATRIX - AVAILABLE NOW!

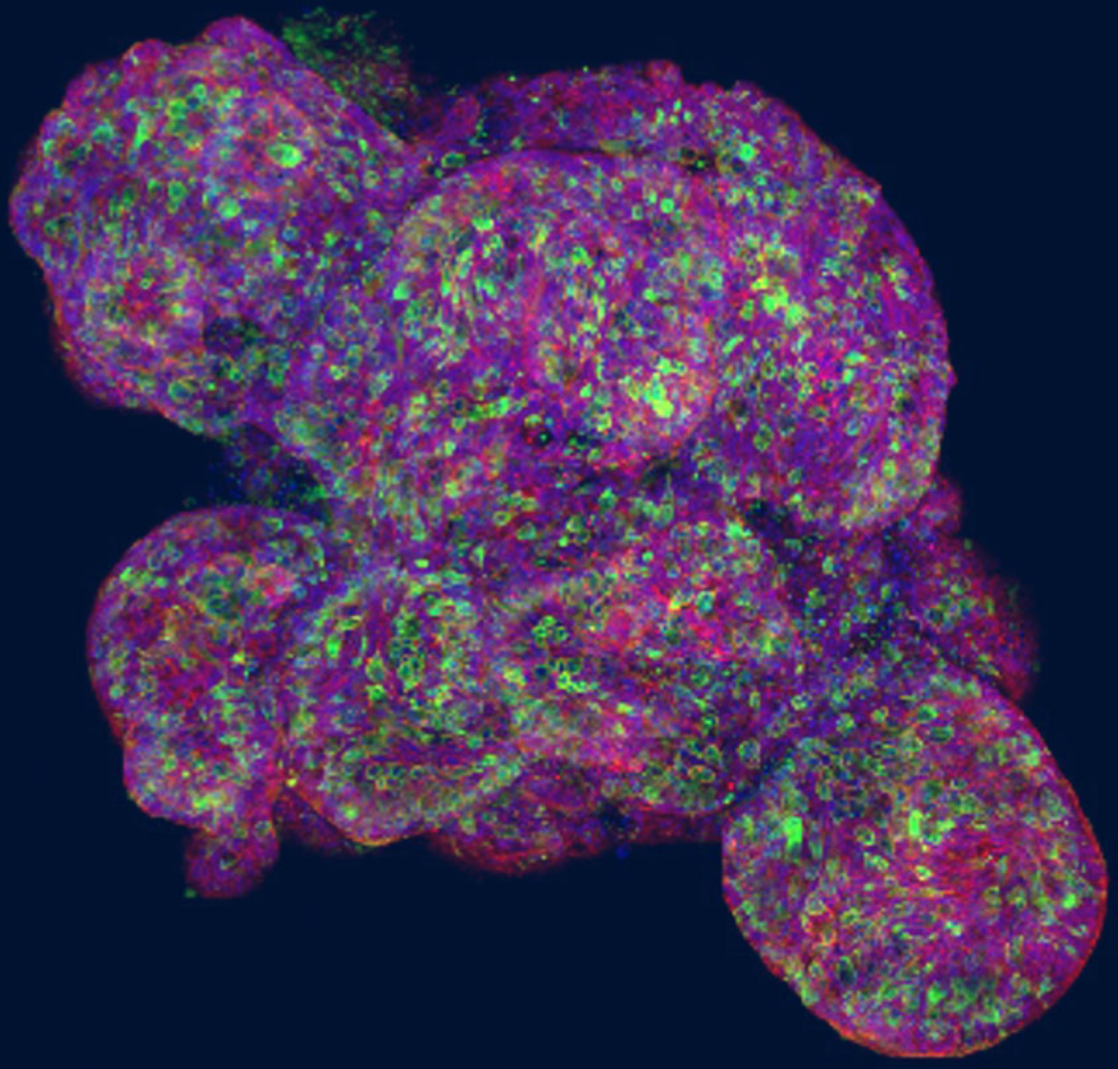

KEY BENEFITS

- Consistent lot-to-lot performance
- Qualified for organoid and pluripotent stem cell culture
- Tensile strength optimized for 3D applications
- Verified for dome formation

PRODUCT FEATURES

- High protein concentration (10-12 mg/mL)
- Enriched in entactin (> 8% of total protein)
- Reduced Growth Factor (RGF) formulation
- Low endotoxin profile (< 7 EU/mL)

Learn more | rndsystems.com/ultimatrix

bio-techne®
bio-techne.com

R&D SYSTEMS NOVUS BIOLOGICALS TOCRIS proteinsimple ACD exosomedx

Global info@bio-techne.com bio-techne.com/find-us/distributors TEL +1 612 379 2956 North America TEL 800 343 7475
Europe | Middle East | Africa TEL +44 (0)1235 529449 China info.cn@bio-techne.com TEL +86 (21) 52380373

STEM CELLS

TISSUE-SPECIFIC STEM CELLS

Gene Expression Profiling Supports the Neural Crest Origin of Adult Rodent Carotid Body Stem Cells and Identifies CD10 as a Marker for Mesectoderm-Committed Progenitors

ELENA NAVARRO-GUERRERO,[a] AIDA PLATERO-LUENGO,[a] PEDRO LINARES-CLEMENTE,[a] ILDEFONSO CASES,[b] JOSÉ LÓPEZ-BARNEO,[a,c] RICARDO PARDAL[a]

Key Words. Adult neural stem cells • Neural crest • Carotid body • Hypoxia • Angiogenesis • CD10

[a]Departamento de Fisiología Médica y Biofísica, Instituto de Biomedicina de Sevilla (IBiS), Hospital Universitario Virgen del Rocío/CSIC/Universidad de Sevilla, Spain; [b]Bioinformatics and Computational Biology Group. Instituto de Biomedicina de Sevilla (IBiS), Hospital Universitario Virgen del Rocío/CSIC/Universidad de Sevilla, Spain; [c]Centro de Investigación Biomédica en Red sobre Enfermedades Neurodegenerativas (CIBERNED), Spain

Correspondence: Ricardo Pardal, Ph.D., Instituto de Biomedicina de Sevilla (IBiS), Hospital Universitario Virgen del Rocío/CSIC/Universidad de Sevilla, Dpto. de Fisiología Médica y Biofísica, Avenida Manuel Siurot s/n, E-41013 Seville, Spain. Telephone: + 34-955-923038; Fax: + 34-955-923101; e-mail: rpardal@us.es

Received April 14, 2015; accepted for publication December 24, 2015; first published online in STEM CELLS *EXPRESS* February 11, 2016.

1066-5099/2016/$30.00/0

http://dx.doi.org/10.1002/stem.2331

ABSTRACT

Neural stem cells (NSCs) are promising tools for understanding nervous system plasticity and repair, but their use is hampered by the lack of markers suitable for their prospective isolation and characterization. The carotid body (CB) contains a population of peripheral NSCs, which support organ growth during acclimatization to hypoxia. We have set up CB neurosphere (NS) cultures enriched in differentiated neuronal (glomus) cells versus undifferentiated progenitors to investigate molecular hallmarks of cell classes within the CB stem cell (CBSC) niche. Microarray gene expression analysis in NS is compatible with CBSCs being neural crest derived-multipotent progenitor cells able to sustain CB growth upon exposure to hypoxia. Moreover, we have identified CD10 as a marker suitable for isolation of a population of CB mesectoderm-committed progenitor cells. CD10 + cells are resting in normoxia, and during hypoxia they are activated to proliferate and to eventually complete maturation into mesectodermal cells, thus participating in the angiogenesis necessary for CB growth. Our results shed light into the molecular and cellular mechanisms involved in CBSC fate choice, favoring a potential use of these cells for cell therapy. STEM CELLS *2016;34:1637–1650*

SIGNIFICANCE STATEMENT

This work extends our work on adult carotid body neural stem cells, which undergo neurogenesis and angiogenesis to contribute to hypoxic acclimatization. Herein, we elucidate mesectodermal differentiation from carotid body stem cells by identifying CD10 as a marker for mesectoderm-committed progenitors in the organ. We offer mechanistic insights and conclude that CD10 contributes to define the onset of angiogenesis in response to hypoxia. Our data shed light on the mechanisms underlying selective carotid body stem cell activation and fate choice. We believe our manuscript is appealing, of technical quality, and should attract the attention of a broad audience of stem cell biologists.

INTRODUCTION

The discovery of adult neural stem cells (NSCs) has provided unprecedented opportunities for studying plasticity and regeneration in the nervous system, as well as for developing new potential therapies for neurological disorders. However, the mechanisms underlying NSC homeostasis are still poorly known. As stem cells in the niches are normally in relatively small numbers and intermingled with other cell types, NSC research is hampered by the lack of specific markers suitable for their identification and prospective isolation. Therefore, studies aiming at the molecular characterization of NSCs in different functional stages are necessary to progress in the understanding of NSC biology and their biomedical applications.

The mammalian central nervous system (CNS) contains two well-identified NSC niches; the subgranular zone in the hippocampus [1], and the subventricular zone (SVZ) lining the lateral ventricles [2]. NSCs within the SVZ are relatively well characterized, and, recently, surface markers suitable for their prospective isolation have been described [3, 4]. Multipotent NSCs also exist in the adult peripheral nervous system (PNS), although their actual physiological role is thus far unknown. [5–7]. An exception is the carotid body (CB), a paired chemoreceptor organ located at the bifurcation of the carotid artery, which contains a

population of neural crest-derived stem cells that support organ growth during acclimatization to sustained hypoxia [8]. The CB is composed of clusters of neuron-like, O_2-sensitive, glomus cells (tyrosine hydroxylase positive [TH+]) enveloped by long processes of glia-like (glial fibrillary acidic protein positive [GFAP+]) type II cells. We have shown that type II cells, or a subpopulation of them, are multipotent stem cells [8, 9]. Glomus cells are presynaptic elements of "chemosensory synapses," which, in response to hypoxia, release transmitters that stimulate sensory fibers activating the respiratory center to elicit hyperventilation [10]. Interestingly, activation of CB stem cells (CBSCs) in hypoxia is not cell autonomous but depends on the O_2-sensitive glomus cells, which form "chemo-proliferative synapses" with type II cells, thus inducing their exit from the quiescent state [11]. Activation of type II cells during hypoxia involves a change of phenotype characterized by the loss of GFAP and conversion into nestin + proliferative intermediate progenitors, which in turn differentiate into glomus cells and other cell types [8, 9]. This switch in expression of cytoskeletal proteins, from GFAP to nestin, closely resembles the activation process in SVZ stem cells [12–15]. However, no cell surface markers have been found for either CBSCs or the intermediate progenitors.

As glomus cells are highly dopaminergic and produce large amounts of the glial cell line-derived neurotrophic factor (GDNF), the CB tissue has been successfully used for intracerebral transplantation in animal models of Parkinson's disease (PD) [16–18]. However, CB autografts on PD patients have demonstrated only modest clinical benefit, probably due, among other factors, to the small amount of tissue in a human CB that is available for transplantation [19]. Hence, expansion of CB tissue in vitro from resident adult stem cells is of major therapeutic interest for PD [8, 20]. CBSCs not only generate neuronal cells but can also give rise to mesectodermal derivatives, such as smooth muscle cells [8]. Therefore, clinical application of CBSCs against PD depends on a better understanding of the molecular mechanisms involved in cell fate choice in CB progenitors.

Our study supports the neural crest origin of CBSCs, provides molecular insight into their biology, and identifies CD10, a common zinc-dependent metalloendoprotease, as a highly selective surface marker for mesectoderm-committed intermediate progenitors in the CB. Pharmacological blockade of mesectodermal differentiation on CBSCs in vitro could help to increase the yield of production of dopamine- and GDNF-containing glomus cells, which could be potentially useful for antiparkinsonian cell therapy.

Results

Comparative Gene Expression Profiling in the CB Stem Cell Niche

Neurospheres (NS) grown from CB progenitors typically have a central core with nestin + and GFAP + undifferentiated cells, and peripheral blebs composed of TH + neuronal cells at the surface of the core [8]. Following previous studies on NSCs [11, 21, 22], we set up culture conditions to favor preferentially proliferation of undifferentiated cells within the core, resulting in NS with almost no blebs (UNDIFF-NS), or differentiation into neuronal cells, resulting in NS full of blebs and with very small cores (DIFF-NS) (Fig. 1A–1D). Differentiation into neuronal cells was achieved by removing endothelin-1 (ET-1) and mitogens from the medium, and by culturing the NS in hypoxic conditions. Indeed, removal of mitogens significantly decreased the diameter of NS cores and increased the size of differentiating blebs (Fig. 1E–1I), confirming the positive effect of mitogens on progenitor cell proliferation at the expense of differentiation [11, 22]. The ratio of differentiated (TH+) versus undifferentiated (nestin+) cells in the two types of NS was determined by immunohistochemistry on thin sections (Fig. 1C, 1D), and by quantitative PCR (Fig. 1J).

To uncover molecular players in the biology of neuronal or undifferentiated progenitor cells in the CB niche, we performed gene expression analysis in UNDIFF-NS versus DIFF-NS cultures using a rat whole-genome Affymetrix 1.0 array. Hierarchical clustering of the expression data from all NS replicates grouped the samples according to their culture condition, indicating high reproducibility of cultures and RNA extraction protocols (Fig. 1K). Several differentially expressed genes were used to confirm the microarray data by quantitative PCR, with consistent results in all cases (Fig. 1L).

To identify genes enriched in undifferentiated or differentiated NS, we applied a stringent filter consisting on statistical significance (false discovery rate (FDR) < 0.01), and at least a 1.5-fold-expression difference (fold change (FCH) > 1.5) between the two samples. These conditions resulted in 835 genes highlighted in the UNDIFF-NS sample, and 1134 genes underlined in the DIFF-NS sample (Fig. 2A). The biological significance of these expression profiles was determined using Ingenuity Pathway Analysis (IPA) software (Ingenuity Systems), which highlights "Categories" (plus "Biofunctions" within those categories) that are significantly represented in the expression data (see "Experimental Procedures"). As expected, categories associated to proliferation, such as "Cancer", "Cellular growth and proliferation", or "Cell cycle", appear in UNDIFF-NS, while categories associated to the neuronal phenotype, such as "Neurological disease", "Behavior", "Molecular transport", or "Nervous system development and function", appear represented in DIFF-NS, demonstrating a clear difference in the nature of CB cells between the two samples (Supporting Information Table S1). The appearance of categories and biofunctions related to a mesectodermal phenotype in the UNDIFF-NS sample (Supporting Information Table S1), such as "Cardiovascular system development and function", "Skeletal and muscular system development and function", "Development of connective and epithelial tissue", or "Proliferation of diverse mesectodermal cells", supports mesectodermal differentiation capacity of CB undifferentiated cells. Regarding specific genes, those selectively up-regulated in DIFF-NS (Supporting Information Table S2) are related to the neuronal phenotype, including neurotransmitter synthetizing enzymes (e.g. *Ddc, Dbh, Th*), neurotransmitter receptors (e.g. *Adora2a, P2ry12, Drd2*), and synapse proteins (e.g. *Syp, Syt4*). In contrast, genes preferentially expressed in UNDIFF-NS (Supporting Information Table S3) are more diverse, including 'typical' proliferation genes such as *Myc*, genes associated to stem cell self-renewal signaling (e.g. *Egfr, Fgfr1, Wnt5a, Pdgfra, Tgfbr2, Fzd1*), or genes like semaphoring 3A (*Sema3a*) associated to cellular movement [23]. Together, these genes define an undifferentiated proliferative and

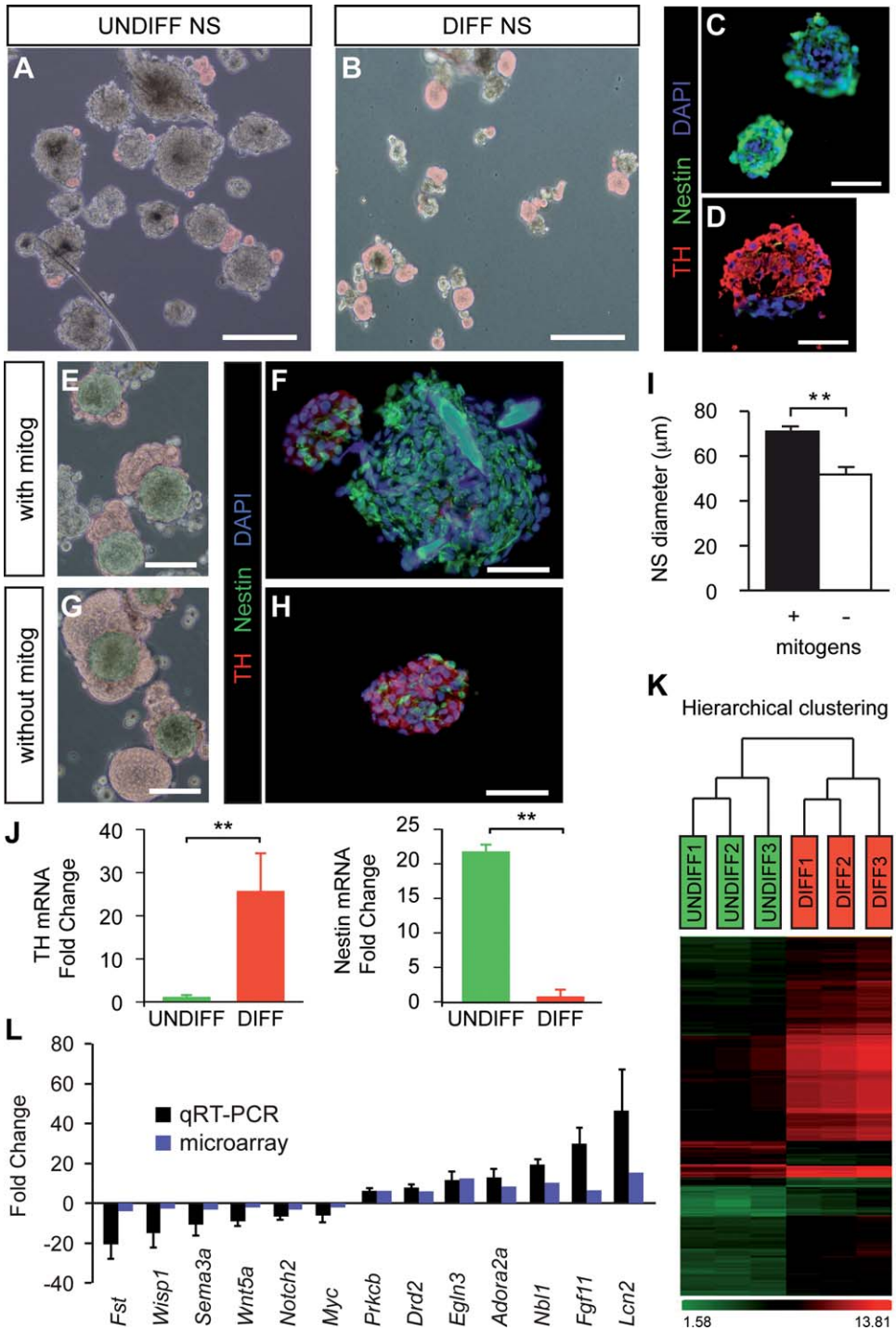

Figure 1. Microarray expression analysis of undifferentiated (UNDIFF) versus differentiated (DIFF) neurospheres (NS). (A and B): Bright field pictures of neurospheres obtained from carotid body (CB) cells cultured in proliferation conditions (medium containing EGF, FGF, IGF, ET1, and 21% O_2; UNDIFF NS; (A)) versus differentiation conditions (without FGF, IGF, EGF, or ET1, and with 3% O_2; DIFF NS; (B)). Neuronal cells (blebs) are pseudocoloured in red. **(C and D)**: Immunohistochemistry of CB undifferentiated (C) and differentiated (D) NS thin sections, stained for TH (red) and nestin (green). Note the high amount of TH + neuronal cells present in the DIFF NS sample, especially when compared to UNDIFF NS, which, on the other hand, are rich in nestin + cells. **(E)**: Bright field image of neurospheres obtained from CB cells cultured with mitogens (EGF, FGF, and IGF). **(F)**: Immunohistochemistry to detect TH (red) and nestin (green) in a thin section of a NS cultured with mitogens. **(G)**: Bright field picture of NS obtained from CB cells cultured without mitogens. **(H)**: Immunohistochemistry to detect TH (red) and nestin (green) in a thin section of a NS cultured without mitogens. **(I)**: Diameter measured in NS cultured with or without mitogens. **(J)**: Relative expression of TH (left) and nestin (right) in undifferentiated versus differentiated NS, studied by qPCR, and confirming the results obtained by histology (C and D). **(K)**: Hierarchical clustering, using the whole set of 27,342 probes, of UNDIFF and DIFF NS samples used for microarray analysis (top), illustrating consistency of the applied culture conditions. Heat-map showing the expression pattern of selected genes (fold change [FCH] > 4 and p value $< .05$) (bottom). **(L)**: Validation of microarray results by qPCR of selected genes. Scale bars, 100 μm in (A, B, E, G), and 50 μm in (C, D, F, H).

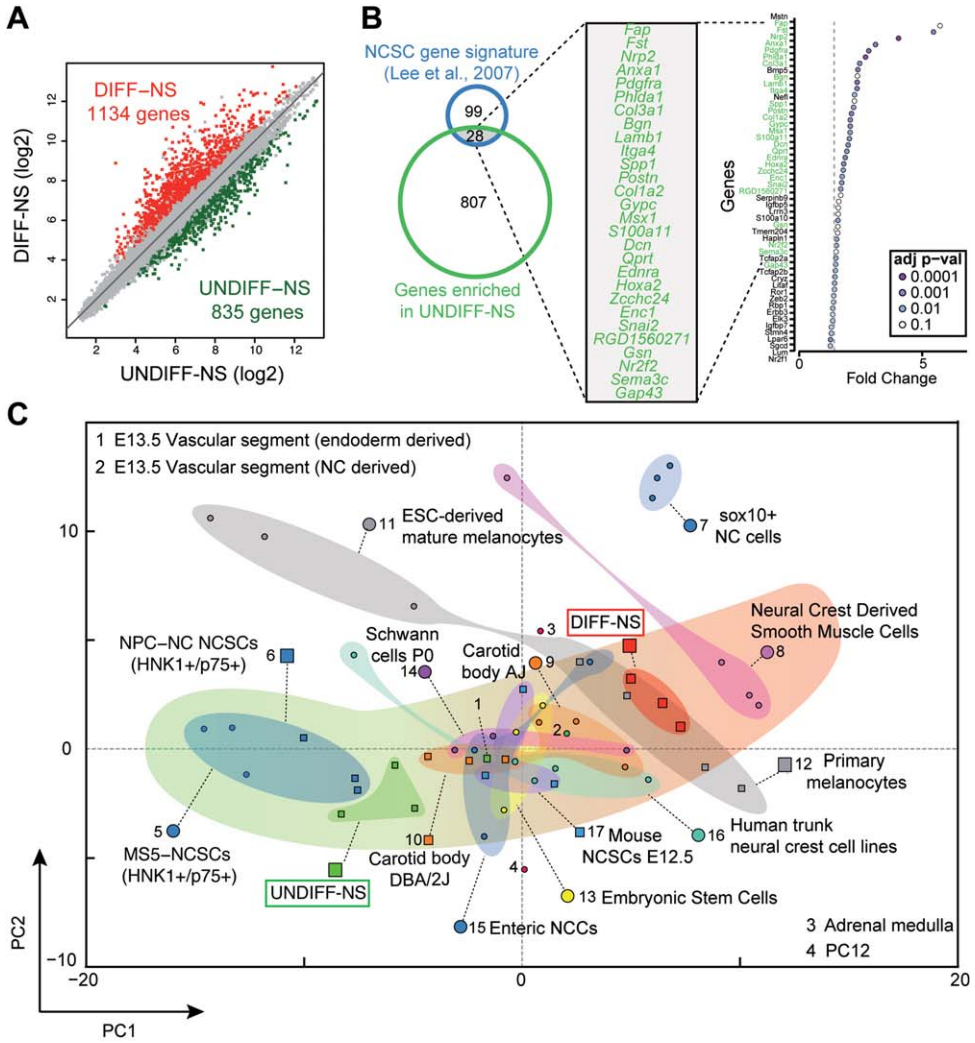

D

Undifferentiated NS	Fold Change
Membrane metallo endopeptidase (*Mme*)	9.07
Hyaluronan synthase2 (*Has2*)	5.14
Receptor activity modifying protein 3 (*Ramp3*)	5.00
Six transmembrane epithelial antigen of the prostate1 (*Steap1*)	4.70
Prostaglandin I2 (prostacyclin) receptor (IP) (*Ptgir*)	4.60
Endothelin receptor type B (*Ednrb*)	4.56

Differentiated NS	Fold Change
Endothelin converting enzyme-like1 (*Ecel1*)	11.68
Purinergic receptor P2Y, G-protein coupled, 12 (*P2ry12*)	10.45
Adenosin A2a receptor (*Adora2a*)	10.12
Adhesion molecule with Ig like domain 2 (*Amigo2*)	7.82
Neurotrophic tyrosine kinase, receptor, type 2 (*Ntrk2*)	6.88
Synaptotagmin XIII (*Syt13*)	6.68

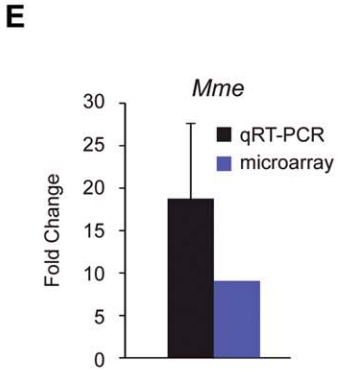

Figure 2. Gene expression analysis supports the neural crest origin of adult carotid body stem cells. (A): Scatter plot of differentially expressed probesets in UNDIFF and DIFF neurospheres, showing in color differentially expressed genes obtained with a false discovery rate (q value) < 0.01 and a fold change >1.5. **(B)**: Overlapping study of UNDIFF-NS enriched cells with human neural crest-derived stem cell (NCSC) signature. **(C)**: Principal Component Analysis comparing UNDIFF-NS and DIFF-NS microarray data with different neural crest cell microarray data sets (see references in Supporting Information Table S4). Shadows in different colors have been drawn to join similar samples. A background shadow changing from green color (undifferentiation) to reddish color (differentiation) has been drawn following the axis of differentiation status. **(D)**: Table showing the top differentially expressed probesets of membrane proteins in UNDIFF and DIFF NS samples. **(E)**: Confirmation by qPCR of the difference in CD10 gene (*Mme*) expression observed in the microarray between DIFF and UNDIFF samples. Abbreviations: UNDIFF, undifferentiated; DIFF, differentiated; NS, neurospheres.

mobile cell phenotype in the UNDIFF-NS sample, fully compatible with neural crest-derived stem cells (NCSCs) (Supporting Information Table S3).

Cell fate mapping with genetic markers has shown that CBSCs derive from the neural crest [8]. However, their genetic profile has never been compared to other neural crest cells. An important objective in the present study was to uphold the neural crest origin of CB undifferentiated cells. We first compared UNDIFF-NS enriched genes to a specific gene signature for human neural crest-derived stem cells defined by using differentiation from embryonic stem cells [24]. Out of the 127 homologous genes present in this signature, 28 of them are enriched (FCH$>$1.5; p value $<$ .01) in UNDIFF-NS cells (Fig. 2B), a similarity that is significantly nonstochastic ($p <$ .001). The list includes relevant genes for the development and function of the neural crest, such as *Ednra, Hoxa2, Snai2*, etc. This comparison suggests that UNDIFF-NS cells are indeed neural crest-derived. To further relate CB cells to different populations of neural crest cells, we compared the transcriptome-wide profile of both UNDIFF-NS and DIFF-NS cells with publicly available microarray expression data sets from different neural crest cell populations (Supporting Information Table S4). Unbiased principal component analysis (Fig. 2C) revealed that CB cells are similar to other neural crest cell populations. Interestingly, the different cell populations appeared ordered by differentiation status, with undifferentiated cells more to the left of the graph (green color of the background shadow), and more differentiated cells to the right (reddish color of the background shadow). Consistently, UNDIFF-NS samples appear to the left, next to NCSC populations, while DIFF-NS cells appear to the right, next to smooth muscle cells and melanocytes (Fig. 2C). Whole CB samples, which include both progenitors and neuronal cells among other cell types, appear in the middle of the graph. Hence, our *in silico* comparison analysis supports the neural crest origin of CB cells and reinforces the difference in differentiation status between UNDIFF-NS and DIFF-NS cells.

We also focused our study on finding selective cell surface markers that would allow the prospective isolation by flow cytometry of specific cell populations. To this end, we selected the most expressed plasma membrane proteins in the two samples (Fig. 2D). In DIFF-NS these are neurotransmitter and neurotrophic factor receptors, as well as adhesion (Amigo2), and synapse-related (synaptotagmin XIII, Ecel1) proteins. In UNDIFF-NS, the most highly expressed plasma membrane protein, whose level of mRNA expression was confirmed by PCR (Fig. 2E), is a metallo endopeptidase (CD10, encoded by *Mme* gene). The other highly expressed genes encoded proteins involved in the production of extracellular components (Has2) or membrane receptors (Ramp3, Steap1, and Ptgir). Interestingly, UNDIFF-NS samples showed high levels of ET-1 receptor type B mRNA, which is in fair agreement with the role of ET-1 and its receptors in the activation of CB progenitors during adaptation to hypoxia [11, 25]. Among the antibodies tested against these membrane proteins, anti-CD10 yielded the most positive results for flow cytometry isolation of cells in the CB niche. This allowed us to identify a specific subpopulation of progenitors within the CB parenchyma that we proceeded to characterize.

CD10 Positive Cells are Committed Progenitors of the Mesectodermal Lineage of CBSCs

Standard immunohistochemical analyses showed the presence of CD10 + cells within the CB parenchyma, usually associated to blood vessels (Fig. 3A). To determine whether these cells belong to the germinal lineage of CBSCs, we used GFAP-cre/floxed LacZ transgenic mice to perform a cell fate mapping in vivo. We have previously used this transgenic system to label GFAP + CBSCs and their neuronal or mesectodermal progeny [8]. Ex vivo analysis of dispersed CB cells from GFAP-cre/floxed LacZ transgenic mice revealed the presence of β-galactosidase expressing CD10 + cells (Fig. 3B), confirming that these cells are derived from GFAP + CBSCs. Furthermore, we also analyzed the coexpression of CD10 with other markers of CBSC germinal lineage (Fig. 3C–3E). None of CB TH + cells expressed CD10 (Figure 3D–3F), however we found double positive cells for CD10 with GFAP, nestin, smooth muscle actin (SMA), and the endothelium-specific markers lectin (GSA I) and CD31. About 26.75 $\pm$ 4.95% and 3.6 $\pm$ 0.6% of CD10 + cells were also positive for GSA I and CD31 respectively, suggesting that a subpopulation of endothelial cells express the endopeptidase (Figure 3G–3I). Since we have previous data in the group confirming the capacity of CBSCs to differentiate into vascular endothelial cells (Annese et al., unpublished), altogether the coexpression data indicate an association of CD10 with the mesectodermal lineage of CBSCs.

Flow cytometry analyses revealed that 18.8% $\pm$ 1.5% ($n = 10$) of cells in the CB express CD10 (dot plot in Fig. 4A), and when these CD10 + cells were separated by fluorescence-activated cell sorting (FACS), a $>$3-fold increase in the efficiency of NS formation was observed when compared to cultures of CD10− cells (1.79% $\pm$ 0.19% in CD10 + cells vs. 0.54% $\pm$ 0.10% in CD10− cells; $p <$ .01) (Fig. 4B, 4C). Moreover, CD10 + cell-derived NS had a significantly larger diameter than those obtained from CD10− cells (67.3 $\pm$ 2.4 μm vs. 51.8 $\pm$ 1.7 μm; $p <$ .05) (Fig. 4D). However, differentiation studies demonstrated the lack of peripheral blebs of TH + cells within NS derived from CD10 + cells (Fig. 4E–4H). In contrast, mesectodermal differentiation, studied by immunocytochemistry in adherent NS (Fig. 4G), was indistinguishable between CD10 + and CD10− cell-derived NS (Fig. 4I, 4J). These results suggest that, similar to CD10− multipotent cells, CD10 + progenitors can differentiate into mesectodermal lineage, but in this case have lost the potential to differentiate into neuronal lineage. To further distinguish the phenotype of NS cells from CD10 + and CD10− progenitors, we performed qPCRs with genes described in the literature as expressed in neural crest-derived mesectodermal cells (green arrowheads in Fig. 4K) [24, 26–33] or in neural crest-derived neural cells (red arrowheads in Fig. 4K) [24, 29, 30, 33–36]. As expected, mesectodermal genes are preferentially expressed in CD10 + cell-derived NS, while neural genes are preferentially expressed in CD10− cell-derived NS (Fig. 4K), corroborating the mesectodermal commitment of CD10 + progenitor cells. Genes described as expressed by neural crest stem cells [24] are labeled in blue in Fig. 4K, and their expression is distributed throughout both samples, supporting once more the neural crest origin of these cells. Hence, CD10 seems to label a subpopulation of mesectoderm-committed progenitor cells within the CB parenchyma.

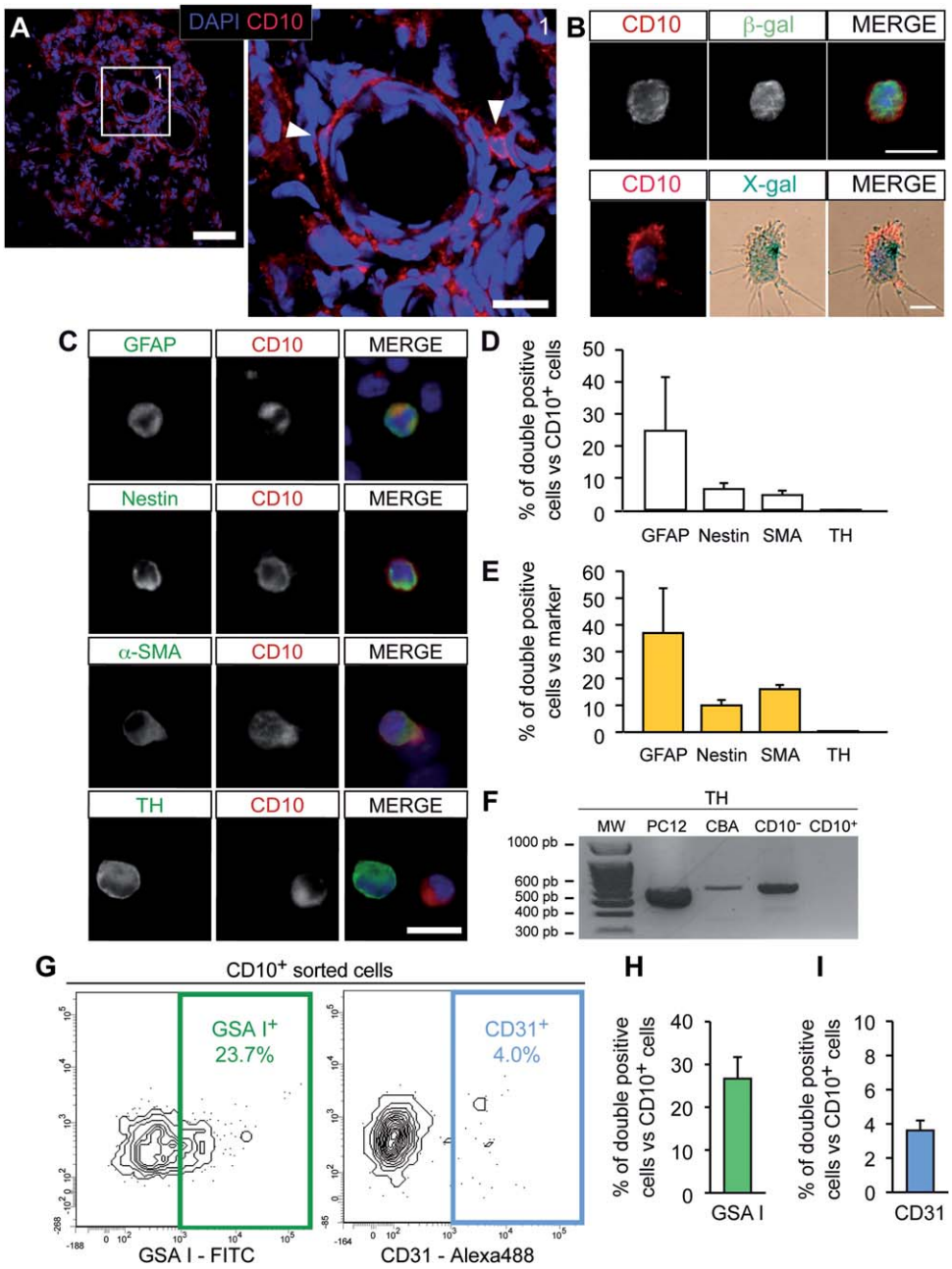

Figure 3. Immunodetection and characterization of CD10 expression in the carotid body (CB). (A): Immunohistochemistry for CD10 (red) in rat CB, showing details of a magnified area (1). Note the proximity of CD10 + cells (arrowheads) to blood vessels. **(B)**: Immunocytochemistry of dispersed CB cells from GFAP-cre/floxed LacZ transgenic mice to perform cell-fate mapping analyses, which corroborate that CD10 + cells lie within the CB progenitor lineage. **(C)**: Example of an immunocytochemistry used for the quantifications shown in (D) and (E). **(D)**: Quantification of cells coexpressing CD10 with other markers, obtained by immunocytochemistry on whole rat CB dispersed cells. **(E)**: Percentage of CD10 + cells within GFAP+, nestin+, SMA+, or TH + cell populations. **(F)**: PCR analysis showing TH expression in PC12, whole CB (CBA), and sorted CD10− and CD10 + CB cells. PCR bands show that CD10 + cells do not express TH. **(G)**: Representative dot-plots of sorted CD10 + CB cells showing coexpression of GSA I (left) and CD31 (right). **(H and I)**: Quantification of GSA I + (H) and CD31 + (I) cells analyzed by flow cytometry within the CD10 + cell population. Altogether, tissue expression and ex vivo cellular coexpression data suggest that CD10 is associated to the mesectodermal lineage progression of CB stem cells. Scale bars, 50 μm in (A), and 10 μm in (B and C). Abbreviations: MW, molecular weight.

Inhibition of CD10 Activates Mesectoderm-Committed Progenitors to Generate Vascular Cell Types

In several cell types, CD10 is known to participate in the cleavage of signaling peptides, making the cells insensitive to low concentrations of these signals [37], along with modulation of intracellular signaling [38]. Therefore, we investigated whether inhibition of this protein altered the function of CB progenitors expressing CD10. Addition of DL-Thiorphan, a pharmacological inhibitor of CD10 endopeptidase activity [39], to CD10− or CD10 + cell-derived NS resulted in an increase in the number of CD10 + cell-derived NS with a slight,

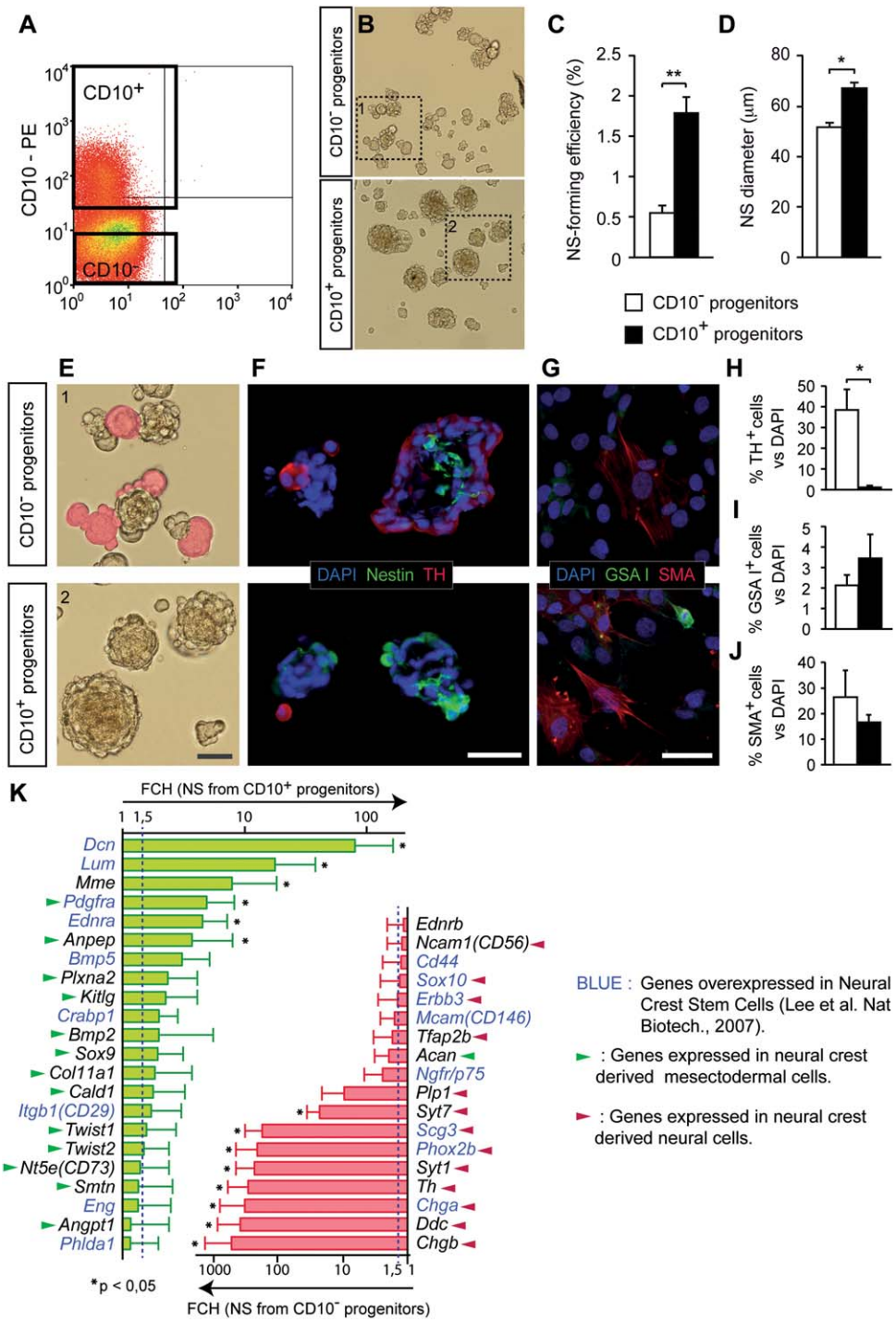

Figure 4. Characterization of CD10 positive progenitors in vitro. (A): Dot-plot showing detection of CD10 + cells in rat CB by flow cytometry. **(B)**: Bright field pictures of neurospheres obtained in culture from CD10− and CD10 + FACS-sorted cells. **(C)**: Neurosphere-forming efficiency of CD10− and CD10 + cells. Note the enrichment in neurosphere-forming cells when sorting for CD10. **(D)**: Diameter measured in NS obtained from CD10− and CD10 + cells. Note how CD10 + cells give rise to bigger neurospheres, suggesting that these progenitors have a higher proliferation capacity than CD10− ones. **(E)**: Details of areas squared in (B). Differentiating blebs are pseudo-colored in red. **(F)**: Immunohistochemistry of CD10− and CD10 + cell-derived NS thin sections, stained for nestin (green) and TH (red). **(G)**: Immunocytochemistry for Lectin (GSA I; green) and SMA (red) performed in adherent NS obtained from CD10− or CD10 + progenitors. **(H)**: Quantification of TH + cells within NS sections, illustrating how CD10 + progenitor cells have lost the ability to differentiate into TH + neuronal cells. **(I and J)**: Quantification of GSA I + (I) and SMA + (J) cells in adherent NS obtained from CD10− or CD10 + progenitors. **(K)**: Quantitative PCRs comparing gene expression of CD10 + cell-derived NS versus CD10− cell-derived NS. Genes were chosen according to their relationship to the neural crest. Note how mesectodermal genes tend to be expressed preferentially in CD10 + progenitor-derived NS samples while neural genes are preferentially expressed in CD10− progenitor-derived NS. Altogether, these data suggest that CD10 + progenitors are committed to the mesectodermal lineage. * $p \leq .05$; ** $p \leq .01$. Scale bars, 50 μm. Abbreviations: FCH, fold change.

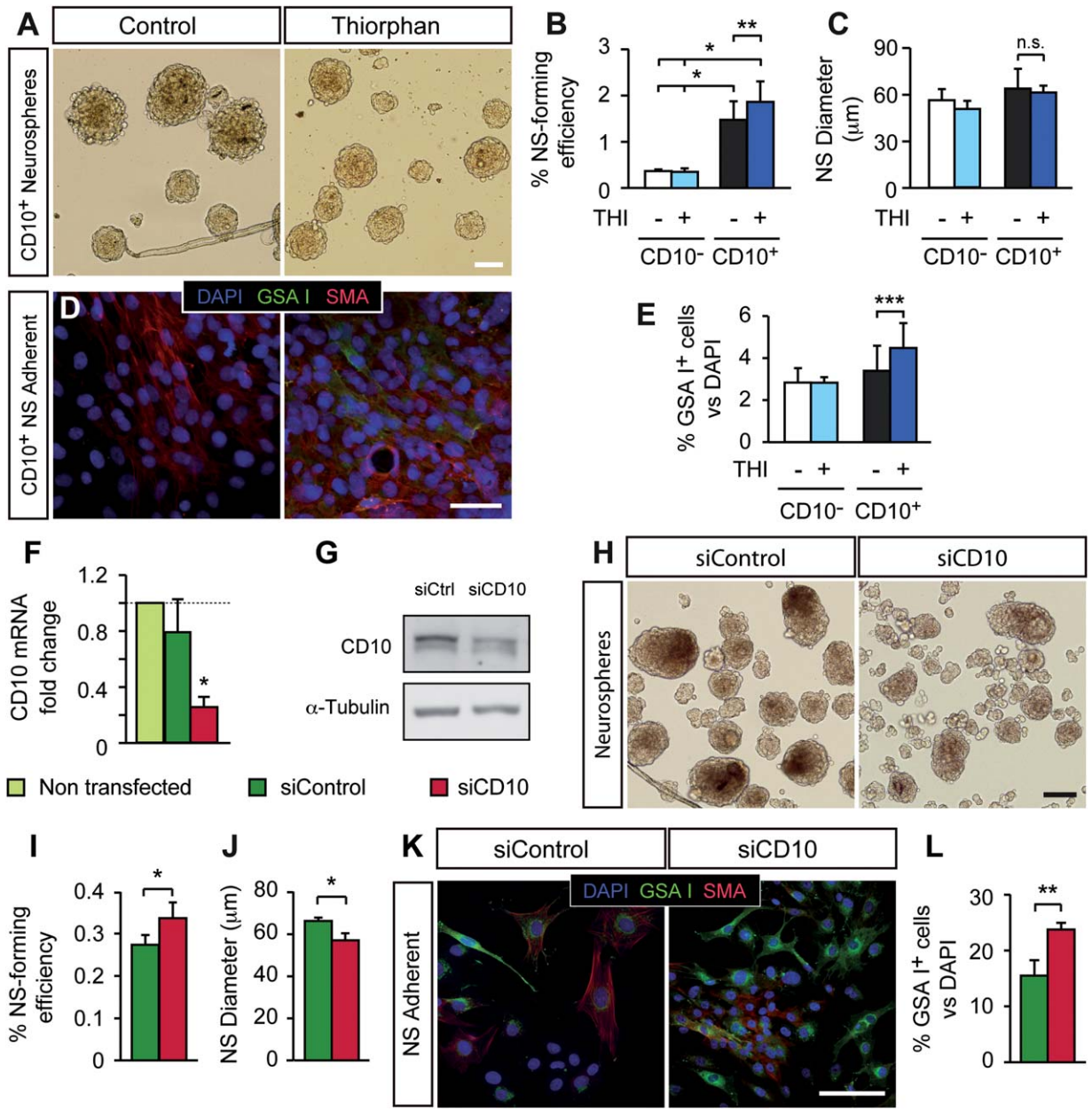

Figure 5. Role of CD10 on carotid body stem cell differentiation. (A): Bright field pictures of NS obtained in culture from CD10 + cells sorted by FACS, and treated or not with CD10 inhibitor DL-Thiorphan (10 μM). Note the enrichment in NS-forming cells in the presence of Thiorphan. **(B)**: NS-forming efficiency of CD10− and CD10 + cells cultured with or without Thiorphan. **(C)**: Diameter measured in CD10− and CD10 + NS. **(D)**: Immunocytochemistry for GSA I (green) and SMA (red) performed in adherent NS obtained from CD10 + progenitors, cultured with or without Thiorphan. **(E)**: Quantification of GSA I + cells in NS obtained as explained in (D). Note how Thiorphan does not affect CD10− progenitors, rather the observed effect is specific for CD10 + progenitors. **(F)**: Quantitative PCR showing relative expression of CD10, 48h after downregulation by siRNAs (50 nM of siControl or siCD10) in cultured CB cells. 50nM siRNA was chosen for subsequent experiments since it produced the highest downregulation without damage to the cells. Data was normalized to relative expression of CD10 in non-transfected cells. **(G)**: Western blot analysis of CD10 in transfected cells. **(H)**: Representative bright field pictures of neurospheres transfected with the indicated siRNA. **(I and J)**: Quantification of NS-forming efficiency (I) and diameter (J) in NS from experiments shown in (H). **(K)**: Immunocytochemistry to detect GSA I (green) and SMA (red), performed in adherent NS from (H). **(L)**: Quantification of GSA I + cells from experiments shown in (K). * $p \leq .05$; ** $p \leq .01$; *** $p \leq .001$; n.s.: non-significant difference. Scale bars, 100 μm in (A, H) and 50 μm in (D, K). Abbreviations: NS, neurospheres; THI, thiorphan.

nonsignificant, decrease in NS diameter (Fig. 5A–5C). Thiorphan also favored mesectodermal differentiation of cells in CD10 + cell-derived NS, cultured in adherent conditions (Fig. 5D, 5E). A similar, but quantitatively stronger, effect on NS-forming efficiency, NS size, and endothelial cell differentiation was observed in preparations treated with siRNA to down-regulate CD10 mRNA (Fig. 5F–5L). These data suggest that CD10 activity contribute to maintain the CD10 + population of mesectoderm-committed progenitors in a resting state, probably through inactivation of mitogenic peptides, such as FGF2 or ET-1, present in the medium [40, 41].

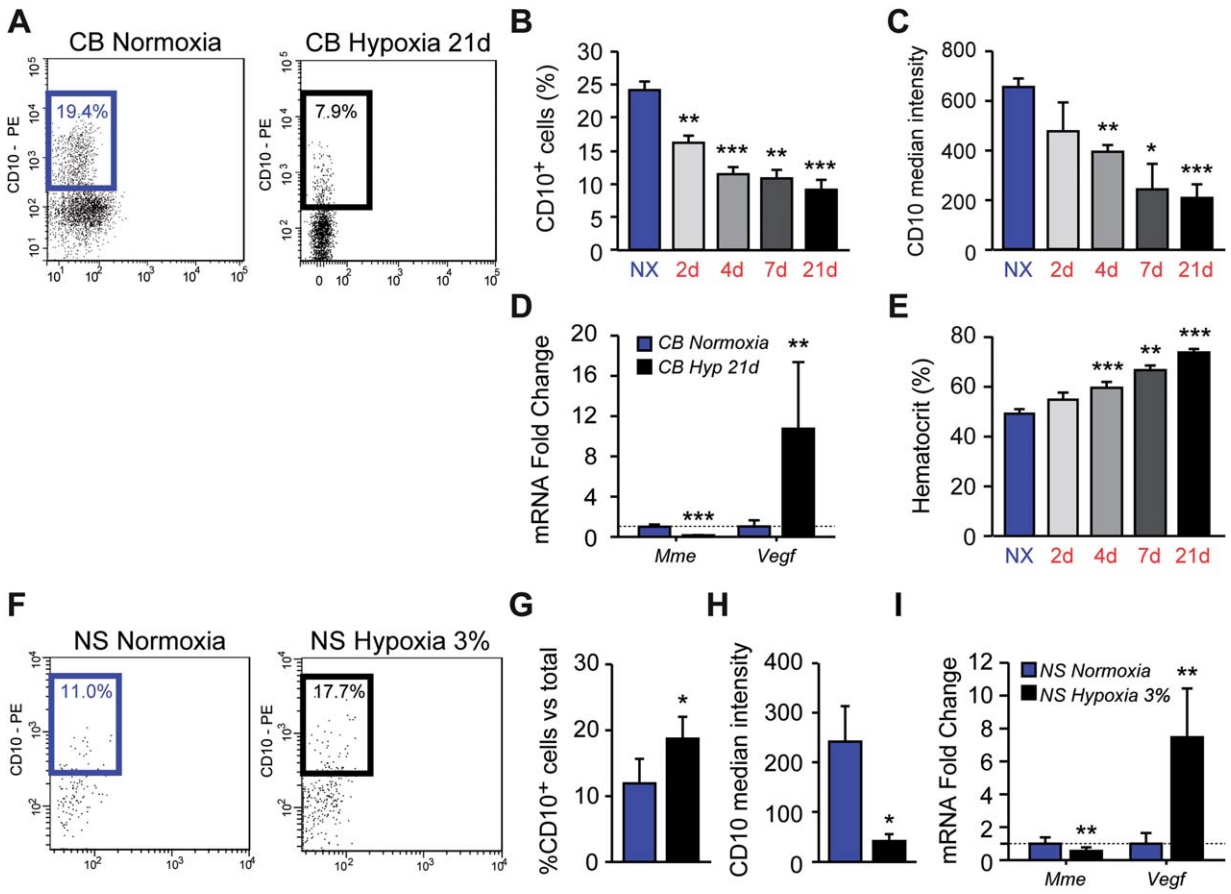

Figure 6. Expression of CD10 is negatively regulated in the rat CB during hypoxia. (**A**): Representative dot-plots showing percentage of CD10 + CB cells from normoxic (Nx, 21% O_2; left) or 21 days-hypoxic (Hx, 10% O_2; right) rats analyzed by FACS. **(B)**: Quantification of CD10 + cells obtained from FACS experiments shown in (A). **(C)**: Median intensity levels of phycoerythrin (PE)-conjugated CD10 in CD10 + cells analyzed in (A and B). These values reflect the expression levels of CD10 in the plasma membrane. Note that both CD10 expression and the number of CD10 + cells decrease at short-time hypoxic exposures, suggesting that CD10 expression is negatively regulated in the CB during hypoxia. **(D)**: Quantitative PCR showing relative expression of *Mme* and *Vegf*, a typical HIF-responsive gene, in normoxic versus 21d-hypoxic whole CB. **(E)**: Quantification of hematocrit in rats exposed to hypoxia (10% O_2), and compared to normoxic rats. **(F)**: Representative FACS dot-plots showing percentage of CD10 + cells in 10d-old neurospheres cultured in normoxic (Nx, 21% O_2) or hypoxic (Hx, 3% O_2) *in vitro* conditions. **(G)**: Quantification of CD10 + cells obtained from FACS experiments shown in (F). **(H)**: Median intensity levels of phycoerythrin (PE)-conjugated CD10 in CD10 + cells analyzed in (F and G). **(I)**: Quantitative PCR showing relative expression of *Mme* and *Vegf* in normoxic and hypoxic neurospheres. * $p \leq .05$; ** $p \leq .01$; *** $p \leq .001$. Abbreviations: CB, carotid body; NS, neurospheres.

We hypothesized that the CD10 + population of progenitors should be much affected by exposure of animals to sustained hypoxia, as this condition is known to produce enlargement of the parenchyma as well as increase in angiogenesis [42–44]. As expected, exposure of rats to hypoxia (10% O_2 tension) produced a time-dependent decrease in the number of CD10 + cells in the CB as well as in the content of CD10 protein within positive cells (Fig. 6A–6C). Regular PCR also showed a clear decrease of *Mme* expression in cells from hypoxic animals (Fig. 6D). Correct exposure to hypoxia was confirmed by increased expression of a typical HIF-dependent gene, vascular endothelial growth factor (*Vegf*; Fig. 6D), and by increased hematocrit measurements in hypoxic animals (Figure 6E). Although NS in vitro seem to display higher percentage of CD10 + cells when exposed to hypoxia (Fig. 6F, 6G), these hypoxic CD10 + cells clearly display lower levels of CD10 in the plasma membrane (Fig. 6H), provoked by a decreased expression of *Mme* mRNA in hypoxic NS cells (Fig. 6I). In vitro exposure to hypoxia was also confirmed by an increased expression of *Vegf* (Fig. 6I). Hence, hypoxia downregulation of CD10 in CB might facilitate activation of mesectodermal progenitors and their maturation into vascular cells.

ET-1 Induces Mesectodermal Differentiation in the CB

ET-1 is a pro-proliferation agent that is involved in the regulation of mesenchymal differentiation and angiogenesis in different tissues including the CB [25, 45]. In addition, we have previously shown a strong positive effect of ET-1 on the proliferation of multipotent CB progenitors [11]. Treatment of CB-derived NS with ET-1 increases the diameter of the NS (Fig. 7A) and the proportion of CD10 + progenitors when compared to non-treated controls (from $15.4 \pm 2.7\%$ to $26.2\% \pm 3.3\%$, $p < .001$) (Fig. 7B). The increase in CD10 expression within ET-1 treated NS was also clearly observed at the level of mRNA (Fig. 7C). However, ET-1 treatment did not seem to increase mesectodermal differentiation (number of GSA I + endothelial cells) within NS (Fig. 7D, 7E), although a clear increase in CD10 + cells was confirmed in these

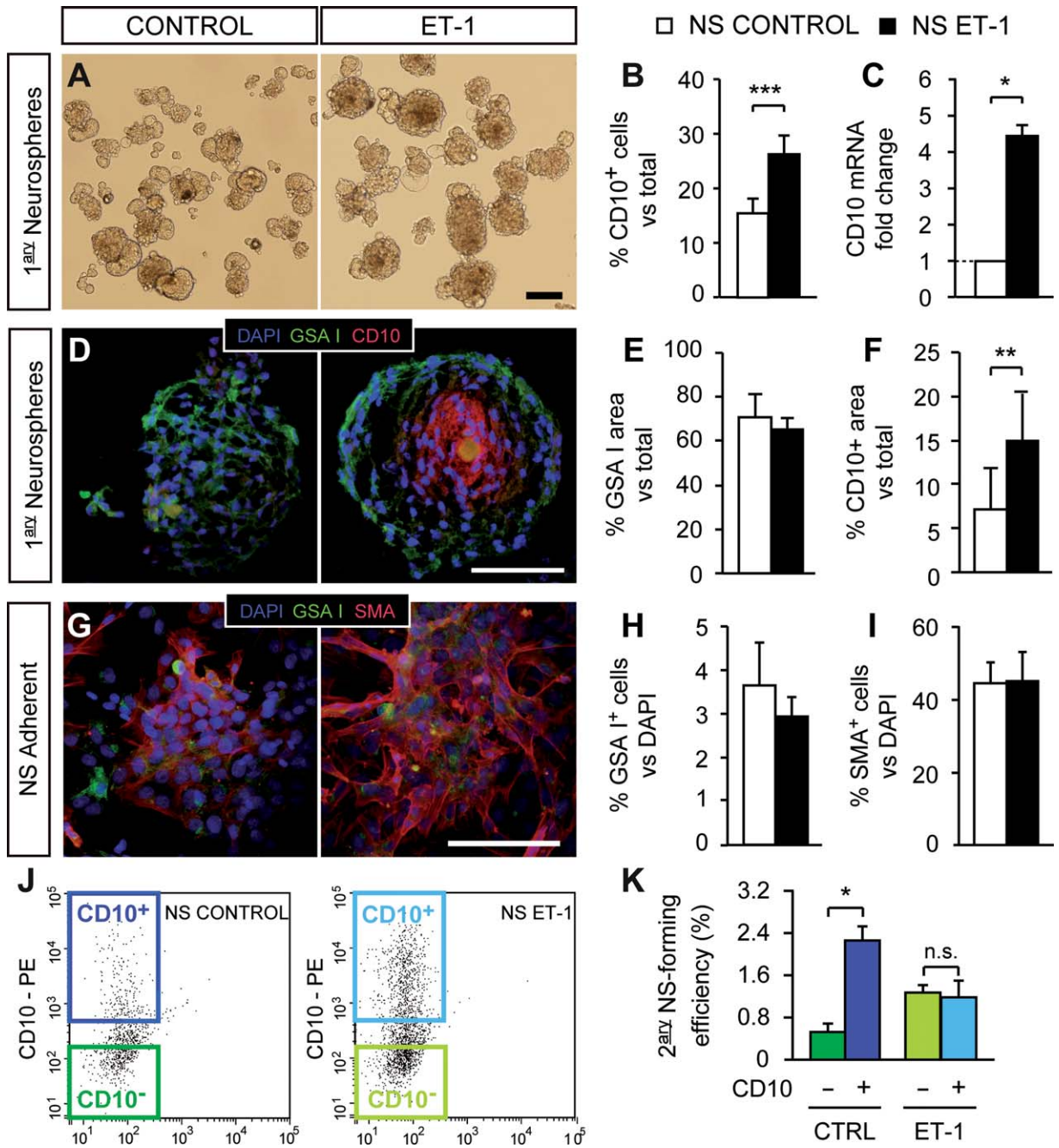

Figure 7. Endothelin-1 promotes mesectodermal lineage by increasing the number of CD10 + cells. (A): Bright field pictures of NS obtained in culture from CB cells treated or not with Endothelin-1 (ET-1). **(B)**: FACS quantification of CD10 + cells in dispersed NS, obtained as in (A). Note the increase in CD10 + cells when NS are treated with ET-1. **(C)**: Quantitative PCR showing higher expression of CD10 in ET-1-treated NS compared to control ones. **(D)**: Immunocytochemistry of thin sections of NS from (A), stained for GSA I (green) and CD10 (red). **(E and F)**: Quantification of positive area for GSA I (E) and CD10 (F) in NS sections as shown in (D). **(G)**: Immunocytochemistry performed in control and ET-1-treated NS cultured in adherent conditions, and stained for GSA I (green) and SMA (red). **(H and I)**: Quantification of the amount of GSA I + (H) and SMA + (I) cells in adherent NS treated or not with ET-1. **(J)**: Representative FACS dot-plots showing CD10 + and CD10− cells from control and ET-1-treated NS. Note the increase in CD10 + cells when NS are treated with ET-1. **(K)**: Secondary NS-forming efficiency of CD10− and CD10 + sorted cells from NS shown in (A). Note the decrease of NS-forming cells within the CD10 + population when NS are cultured with ET-1, indicating that these CD10 + cells have undergone mesectodermal differentiation. * $p \leq .05$; ** $p \leq .01$; *** $p \leq .001$. Scale bars, 100 μm in (A and D) and 50 μm in (G). Abbreviations: NS, neurospheres.

immunostained NS thin sections (Fig. 7D, 7F). Mesectodermal differentiation induced by culturing NS in adherent substrate was also unaffected by ET-1 (Fig. 7G–7I). However, this is probably due to the adherent substrate being too strong stimulus for mesectodermal differentiation in all conditions. Interestingly, sorted CD10 + cells from ET-1-treated NS showed a decreased capacity to form NS (Fig. 7J, 7K), suggesting that in fact these cells have undergone mesectodermal

differentiation in response to the vascular cytokine, even though they are not yet mature endothelial cells.

Discussion

In this paper, we report the result of a gene expression analysis performed on the CBSC niche. We have set up conditions to generate differentiated (enriched in neuronal cells) and undifferentiated (enriched in multipotent progenitors) stem cell-derived colonies (NS). The microarray data, and our *in silico* comparison to other neural crest cell profiles, support CBSCs as neural crest-derived multipotent cells. Furthermore, principal component analysis has further established the differences in differentiation status between UNDIFF-NS and DIFF-NS cells. Undifferentiated cells show a gene expression pattern compatible with proliferative and migratory neural crest-derived stem cells [46], thus distinguishing CBSCs from other populations of adult NSCs in the CNS [3, 4]. Our gene expression analysis has identified a number of molecules and signaling pathways potentially important for CBSC biology, which should be further studied in the future. In addition, it has revealed potential surface markers for CB progenitor cells, which could help the development of prospective isolation methods that are not available so far. Indeed, growth as NS has been used as an alternative to elucidate the molecular signature of NSCs [47].

Among the most highly expressed genes encoding membrane proteins in CB undifferentiated cells, we have characterized a zinc-dependent metallo-endopeptidase, named CD10 or neprilysin, which is known to cleave signaling peptides [48, 49] in CNS synapses [48] and in the CB [50, 51]. Although its precise functional role is poorly known, CD10 is widely distributed in human tissues [52], and in a variety of adult stem cell niches [37, 38, 53–55]. Moreover, CD10 has recently gained medical interest as it is expressed by several tumors that present a cancer stem cell phenotype [56–58], and has been used as a diagnostic marker in some solid tumors with strong metastatic potential [59]. We have shown that CD10 is highly expressed in a subpopulation of NS-forming mesectoderm-committed progenitors in the CB. Our data suggest that neprilysin maintains these cells in a "resting" condition characterized by active degradation of pro-angiogenic cytokines, therefore inhibiting angiogenesis. These observations are compatible with the anti-angiogenic role described for neprilysin in prostate cancer [60] and in a murine corneal model [40]. Interestingly, we have shown that CD10 is down-regulated during exposure of the animals to hypoxia, which makes CB progenitors more sensitive to the rise in pro-angiogenic cytokines, and facilitates their mesectodermal differentiation and vessel formation. Hence, reduction in CD10 expression contributes to the onset of angiogenesis in the CB and the subsequent adaptation of the organ to sustained hypoxia.

Our in vitro studies also indicate that ET-1 induces the conversion of multipotent CBSCs into CD10 + mesectodermal progenitors. ET-1 is a vascular peptide known to influence the biology of neural crest progenitors during development [61–63]. It is transcriptionally up-regulated by hypoxia and in adult life acts as a potent proliferative agent participating in chronic hypoxia-induced vascular wall thickening, pulmonary hypertension, and right cardiac hypertrophy [64–66]. ET-1 has been suggested to be expressed in the CB to contribute to CB plasticity (growth) under chronic hypoxia [25, 67, 68]. Indeed, we have recently provided unequivocal evidence that ET-1 is produced in CB glomus cells and that participates as a mediator in the O_2-sensitive glomus cell-stem cell chemoproliferative synapse [11]. Hypoxia triggers ET-1 release from glomus cells which binds to receptors in stem cells to induce proliferation [11]. The data presented here indicates that ET-1 released from glomus, and probably also from endothelial, cells increases the number of CD10 + progenitors, which are committed to a mesectodermal fate. In parallel, hypoxia down-regulates protein expression of the metalloendopeptidase, thus facilitating the action of pro-angiogenic cytokines on mesectodermal progenitors, increasing their maturation and the subsequent formation of new blood vessels necessary for CB growth. Taken together, these data shed light on the mechanisms underlying selective CBSC activation supporting CB growth during physiological adaptation to sustained hypoxia. They might also improve our ability to differentially generate dopaminergic and GDNF-producing CB cells usable for cell therapy against PD.

Experimental Procedures

Animals

Transgenic mice, WT mice, and Wistar rats were housed and treated according to the animal care guidelines of the European Community Council (86/609/EEC). All procedures were approved by the Animal Research Committee at the University of Seville.

In Vivo Hypoxic Treatments

Animals (rats and mice) were chronically exposed to a 10% O_2 environment using a hermetic isobaric chamber with O_2 and CO_2 controls and temperature and humidity monitoring (Coy Laboratory Products, Grass Lake, MI; http://www.coylab.com). Animals were maintained in the hypoxic environment for 2, 4, 7, or 21 days. Age-matched control rats were similarly housed in ambient air outside the chamber.

Histo- and Cytochemical Studies

For detection of TH, nestin, α-SMA, CD10, GFAP, GSA I (lectin), and CD31 in tissue sections, NS, and/or dispersed cells, we used standard staining procedures. Specific details about immunocytochemistry, immunohistochemistry, and X-Gal staining are given in the Supplemental Information.

Western Blot

The same quantity of total protein lysate (30 μg) was subjected to 10% SDS-PAGE and transferred onto PVDF membrane, which was incubated with specific antibodies for the detection of CD10, and α-Tubulin as a loading and transfer control. Specific details are given in the Supplemental Information.

Cell Dissociation and Neurosphere Assays

CB cell dissociation and NS assays were performed as described in a previous paper from our laboratory [8]. Specific details are given in the Supplemental Information.

RT-PCR and siRNA Assays

Total RNA was extracted from intact CBs, NS, or dissociated cells using a commercial kit (RNeasy MICRO kit; QIAGEN, Valencia, CA; https://www.qiagen.com). For the extraction, 6–10 CBs, or the equivalent amount of tissue from NS was used. Specific details of the procedures used for standard and real-time quantitative PCR are given in the Supplemental Information. Oligonucleotides are listed in Supporting Information Table S5. Dispersed CB cells were transfected after 8 hour in culture with siRNA smart pools against NEP, or siRNA control smart pool (50 nM; Sigma, St. Louis, MO; https://www.sigmaaldrich.com/), using lipofectamine2000 (Life Technologies-Invitrogen). Cells were allowed to form NS. Specific mRNA downregulation was analyzed 48 hour after transfection by qPCR.

Microarray and IPA Analysis

Expression analysis was performed using GeneChip microarrays Rat Gene 1.0 ST Array (Affymetrix, Santa Clara, CA; http://www.affymetrix.com/) as per manufacturer's instructions. An estimated number of 27.342 annotated genes were analyzed. The data obtained from the microarray analysis were validated by qRT- PCR using TaqMan Array 96-well FAST plate (Applied Biosystems, Waltham, MA; https://www.thermofisher.com/es/es/home.html) containing a group of genes of interest, including endogenous control genes (18S RNA, GAPDH, GUSB, and HRTP1), according to manufacturer's instructions. Statistical analysis of the microarray data was done by LIMMA (Linear Models for Microarray Analysis) using R software, which is recommended for this platform. This analysis applies a t-test empirically adjusted by a Bayes test. All microarray rough analysis files are available from the GEO (http://www.ncbi.nlm.nih.gov/geo) database (accession number GSE67429). To generate expression signatures, we compared UNDIFF-NS to DIFF-NS and selected significant genes (FDR $<$ 0.01), with high FCH, and high average expression ($>$5). To obtain biological significance from genomic data, we used IPA software from Ingenuity System, applying constrain settings (FCH $>$ 1.5 and FDR $<$ 0.01).

Gene enrichment and PCA analysis

In order to calculate the overlapping among genes with affected expression in different conditions, probes were mapped to genes using Array manufacturer annotation. For those human genes with no direct homologous in rats, putative orthologous genes where identified using the Homologene Database [69]. Rat genes were then mapped to probes again using manufacturer annotations. Significance of overlapping was assessed using a two-tailed fisher exact test. For PCA analysis, expression matrices were downloaded from GEO, and a similar process was followed. Probes were mapped to genes using manufacturer provided annotation, and putative orthologous genes in rat were identified using Ensembl (release 82) [70]. Rat genes were in turn mapped to probes in the array. When several original probes were mapped to the same rat gene, values were averaged. All probes not present in all samples were discarded and expression values were transformed to log 2. To remove variation among experiments, a batch effect elimination procedure was applied using the combat function of the sva R package [71].

Flow Cytometry

All sorts and analyses were performed as indicated before [8]. Details on staining and the procedures used are given in the Supplemental Information.

Statistics

Data are given as mean $\pm$ SEM. Statistical significance was estimated by paired or unpaired two-sample *t* test. Paired *t* tests were used to analyze samples obtained from cell cultures, and unpaired *t* tests were applied for the experiments involving animals.

Acknowledgments

This research is supported by grants from the Botín Foundation (JL-B), the Spanish Ministry of Science and Innovation SAF program (JL-B, and RP), and the European Research Council (ERC Starting Grant to RP). We thank M[a] José Castro and Ismael Rodríguez-Prieto for technical assistance.

Authors Contributions

E.N.-G.: Conception and design, collection and/or assembly of data, data analysis and interpretation. A.P.-L.: Conception and design, collection and/or assembly of data, data analysis and interpretation. P.L.-C.: Collection and/or assembly of data, data analysis and interpretation. Ildefonso Cases: Data analysis. J.L.-B.: Conception and design, data analysis and interpretation, financial support, manuscript writing. R.P.: Conception and design, data analysis and interpretation, financial support, manuscript writing. E.N-G. and A.P-L. contributed equally to this work.

Disclosure of Potential Conflicts of Interest

The authors indicate no potential conflicts of interest.

References

1 Eriksson PS, Perfilieva E, Bjork-Eriksson T et al. Neurogenesis in the adult human hippocampus. Nat Med 1998;4:1313–1317.

2 Doetsch F, Caille I, Lim DA et al. Subventricular zone astrocytes are neural stem cells in the adult mammalian brain. Cell 1999;97:703–716.

3 Beckervordersandforth R, Tripathi P, Ninkovic J et al. In vivo fate mapping and expression analysis reveals molecular hallmarks of prospectively isolated adult neural stem cells. Cell Stem Cell 2010;7:744–758.

4 Codega P, Silva-Vargas V, Paul A et al. Prospective identification and purification of quiescent adult neural stem cells from their in vivo niche. Neuron 2014;82:545–559.

5 Morrison SJ, White PM, Zock C et al. Prospective identification, isolation by flow cytometry, and in vivo self-renewal of multipotent mammalian neural crest stem cells. Cell 1999;96:737–749.

6 Kruger GM, Mosher JT, Bixby S et al. Neural crest stem cells persist in the adult gut but undergo changes in self-renewal, neuronal subtype potential, and factor responsiveness. Neuron 2002;35:657–669.

7 Joseph NM, He S, Quintana E et al. Enteric glia are multipotent in culture but primarily form glia in the adult rodent gut. J Clin Invest 2011;121:3398–3411.

8 Pardal R, Ortega-Saenz P, Duran R et al. Glia-like Stem Cells Sustain Physiologic Neu-

rogenesis in the Adult Mammalian Carotid Body. Cell 2007;131:364–377.
9 Macias D, Fernandez-Aguera MC, Bonilla-Henao V et al. Deletion of the von Hippel-Lindau gene causes sympathoadrenal cell death and impairs chemoreceptor-mediated adaptation to hypoxia. EMBO Mol Med 2014;6:1577–1592.
10 Weir EK, Lopez-Barneo J, Buckler KJ et al. Acute oxygen-sensing mechanisms. N Engl J Med 2005;353:2042–2055.
11 Platero-Luengo A, Gonzalez-Granero S, Duran R et al. An O2-sensitive glomus cell-stem cell synapse induces carotid body growth in chronic hypoxia. Cell 2014;156: 291–303.
12 Garcia AD, Doan NB, Imura T et al. GFAP-expressing progenitors are the principal source of constitutive neurogenesis in adult mouse forebrain. Nat Neurosci 2004;7:1233–1241.
13 Seri B, Garcia-Verdugo JM, McEwen BS et al. Astrocytes give rise to new neurons in the adult mammalian hippocampus. The Journal of neuroscience 2001;21:7153–7160.
14 Doetsch F, Petreanu L, Caille I et al. EGF converts transit-amplifying neurogenic precursors in the adult brain into multipotent stem cells. Neuron 2002;36:1021–1034.
15 Doetsch F. The glial identity of neural stem cells. Nat Neurosci 2003;6:1127–1134.
16 Munoz-Manchado AB, Villadiego J, Suarez-Luna N et al. Neuroprotective and reparative effects of carotid body grafts in a chronic MPTP model of Parkinson's disease. Neurobiol Aging 2013;34:902–915.
17 Toledo-Aral JJ, Méndez-Ferrer S, Pardal R et al. Trophic restoration of the nigrostriatal dopaminergic pathway in long-term carotid body-grafted parkinsonian rats. J Neurosci 2003;23:141–148.
18 Villadiego J, Mendez-Ferrer S, Valdes-Sanchez T et al. Selective glial cell line-derived neurotrophic factor production in adult dopaminergic carotid body cells in situ and after intrastriatal transplantation. J Neurosci 2005;25:4091–4098.
19 Minguez-Castellanos A, Escamilla-Sevilla F, Hotton GR et al. Carotid body autotransplantation in Parkinson disease: A clinical and positron emission tomography study. J Neurol Neurosurg Psychiatry 2007;78:825–831.
20 Ortega-Saenz P, Pardal R, Levitsky K et al. Cellular properties and chemosensory responses of the human carotid body. J Physiol 2013;591:6157–6173.
21 Morrison SJ, Csete M, Groves AK et al. Culture in reduced levels of oxygen promotes clonogenic sympathoadrenal differentiation by isolated neural crest stem cells. J Neurosci 2000;20:7370–7376.
22 Schwindt TT, Motta FL, Barnabe GF et al. Short-term withdrawal of mitogens prior to plating increases neuronal differentiation of human neural precursor cells. PLoS One. 2009;4:e4642.
23 Kawasaki T, Bekku Y, Suto F et al. Requirement of neuropilin 1-mediated Sema3A signals in patterning of the sympathetic nervous system. Development 2002; 129:671–680.
24 Lee G, Kim H, Elkabetz Y et al. Isolation and directed differentiation of neural crest stem cells derived from human embryonic stem cells. Nat Biotechnol 2007;25:1468–1475.
25 Chen J, He L, Dinger B et al. Role of endothelin and endothelin A-type receptor in adaptation of the carotid body to chronic hypoxia. Am J Physiol 2002;282:L1314–1323.
26 Cheung C, Goh YT, Zhang J et al. Modeling cerebrovascular pathophysiology in amyloid-beta metabolism using neural-crest-derived smooth muscle cells. Cell Rep 2014; 9:391–401.
27 Fukuta M, Nakai Y, Kirino K et al. Derivation of mesenchymal stromal cells from pluripotent stem cells through a neural crest lineage using small molecule compounds with defined media. PLoS One 2014;9: e112291.
28 Isenmann S, Arthur A, Zannettino AC et al. TWIST family of basic helix-loop-helix transcription factors mediate human mesenchymal stem cell growth and commitment. Stem Cells 2009;27:2457–2468.
29 Isern J, Garcia-Garcia A, Martin AM et al. The neural crest is a source of mesenchymal stem cells with specialized hematopoietic stem cell niche function. Elife 2014;3: e03696.
30 John N, Cinelli P, Wegner M et al. Transforming growth factor beta-mediated Sox10 suppression controls mesenchymal progenitor generation in neural crest stem cells. Stem Cells 2011;29:689–699.
31 Simoes-Costa M, Tan-Cabugao J, Antoshechkin I et al. Transcriptome analysis reveals novel players in the cranial neural crest gene regulatory network. Genome Res 2014;24:281–290.
32 Umeda K, Oda H, Yan Q et al. Long-term expandable SOX9 + chondrogenic ectomesenchymal cells from human pluripotent stem cells. Stem Cell Reports 2015;4:712–726.
33 Vincentz JW, Firulli BA, Lin A et al. Twist1 controls a cell-specification switch governing cell fate decisions within the cardiac neural crest. PLoS Genet 2013;9: e1003405.
34 Daubner SC, Le T, Wang S. Tyrosine hydroxylase and regulation of dopamine synthesis. Arch Biochem Biophys 2011;508:1–12.
35 Langley K, Grant NJ. Molecular markers of sympathoadrenal cells. Cell Tissue Res 1999;298:185–206.
36 Segovia M, Ales E, Montes MA et al. Push-and-pull regulation of the fusion pore by synaptotagmin-7. Proc Natl Acad Sci USA 2010;107:19032–19037.
37 Bachelard-Cascales E, Chapellier M, Delay E et al. The CD10 enzyme is a key player to identify and regulate human mammary stem cells. Stem Cells 2010;28:1081–1088.
38 Maguer-Satta V, Besancon R, Bachelard-Cascales E. Concise review: Neutral endopeptidase (CD10): A multifaceted environment actor in stem cells, physiological mechanisms, and cancer. Stem Cells 2011;29:389–396.
39 Roques BP, Fournie-Zaluski MC, Soroca E et al. The enkephalinase inhibitor thiorphan shows antinociceptive activity in mice. Nature 1980;288:286–288.
40 Goodman OB, Jr., Febbraio M, Simantov R et al. Neprilysin inhibits angiogenesis via proteolysis of fibroblast growth factor-2. J Biol Chem 2006;281:33597–33605.
41 Karoor V, Oka M, Walchak SJ et al. Neprilysin regulates pulmonary artery smooth muscle cell phenotype through a platelet-derived growth factor receptor-dependent mechanism. Hypertension 2013; 61:921–930.
42 Arias-Stella J, Valcarcel J. Chief cell hyperplasia in the human carotid body at high altitudes; physiologic and pathologic significance. Hum Pathol 1976;7:361–373.
43 Heath D, Smith P, Jago R. Hyperplasia of the carotid body. J Pathol. 1982;138:115–127.
44 Wang ZY, Bisgard GE. Chronic hypoxia-induced morphological and neurochemical changes in the carotid body. Microsc Res Tech 2002;59:168–177.
45 Rubanyi GM, Polokoff MA. Endothelins: Molecular biology, biochemistry, pharmacology, physiology, and pathophysiology. Pharmacol Rev 1994;46:325–415.
46 Gammill LS, Bronner-Fraser M. Genomic analysis of neural crest induction. Development 2002;129:5731–5741.
47 Ramalho-Santos M, Yoon S, Matsuzaki Y et al. "Stemness": Transcriptional profiling of embryonic and adult stem cells. Science 2002;298:597–600.
48 Roques BP, Noble F, Dauge V et al. Neutral endopeptidase 24.11: Structure, inhibition, and experimental and clinical pharmacology. Pharmacol Rev 1993;45:87–146.
49 Turner AJ, Tanzawa K. Mammalian membrane metallopeptidases: NEP, ECE, KELL, and PEX. FASEB J. 1997;11:355–364.
50 Kumar GK, Runold M, Ghai RD et al. Occurrence of neutral endopeptidase activity in the cat carotid body and its significance in chemoreception. Brain Res 1990;517:341–343.
51 Kumar GK, Yu RK, Overholt JL et al. Role of substance P in neutral endopeptidase modulation of hypoxic response of the carotid body. Adv Exp Med Biol. 2000;475: 705–713.
52 Erdos EG, Skidgel RA. Neutral endopeptidase 24.11 (enkephalinase) and related regulators of peptide hormones. FASEB J 1989; 3:145–151.
53 Buhring HJ, Battula VL, Treml S et al. Novel markers for the prospective isolation of human MSC. Ann N Y Acad Sci 2007;1106: 262–271.
54 Galy A, Morel F, Hill B et al. Hematopoietic progenitor cells of lymphocytes and dendritic cells. J Immunother 1998;21:132–141.
55 Stingl J, Eaves CJ, Kuusk U et al. Phenotypic and functional characterization in vitro of a multipotent epithelial cell present in the normal adult human breast. Differentiation 1998;63:201–213.
56 Clarke MF, Dick JE, Dirks PB et al. Cancer stem cells–perspectives on current status and future directions: AACR Workshop on cancer stem cells. Cancer Res 2006;66:9339–9344.
57 Polyak K, Hahn WC. Roots and stems: Stem cells in cancer. Nat Med 2006;12:296–300.
58 Fukusumi T, Ishii H, Konno M et al. CD10 as a novel marker of therapeutic resistance and cancer stem cells in head and neck

squamous cell carcinoma. Br J Cancer 2014; 111:506–514.

59 Chu P, Arber DA. Paraffin-section detection of CD10 in 505 nonhematopoietic neoplasms. Frequent expression in renal cell carcinoma and endometrial stromal sarcoma. Am J Clin Pathol 2000;113:374–382.

60 Horiguchi A, Chen DY, Goodman OB, Jr. et al. Neutral endopeptidase inhibits prostate cancer tumorigenesis by reducing FGF-2-mediated angiogenesis. Prostate Cancer Prostatic Dis 2008;11:79–87.

61 Hosoda K, Hammer RE, Richardson JA et al. Targeted and natural (piebald-lethal) mutations of endothelin-B receptor gene produce megacolon associated with spotted coat color in mice. Cell 1994;79:1267–1276.

62 Shin MK, Levorse JM, Ingram RS et al. The temporal requirement for endothelin receptor-B signalling during neural crest development. Nature 1999;402:496–501.

63 Bonano M, Tribulo C, De Calisto J et al. A new role for the Endothelin-1/Endothelin-A receptor signaling during early neural crest specification. Developmental biology 2008;323:114–129.

64 Bonvallet ST, Zamora MR, Hasunuma K et al. BQ123, an ETA-receptor antagonist, attenuates hypoxic pulmonary hypertension in rats. Am J Physiol 1994;266:H1327–1331.

65 Eddahibi S, Raffestin B, Clozel M et al. Protection from pulmonary hypertension with an orally active endothelin receptor antagonist in hypoxic rats. Am J Physiol 1995;268:H828–835.

66 Oparil S, Chen SJ, Meng QC et al. Endothelin-A receptor antagonist prevents acute hypoxia-induced pulmonary hypertension in the rat. Am J Physiol 1995;268:L95–100.

67 McQueen DS, Dashwood MR, Cobb VJ et al. Endothelins and rat carotid body: Autoradiographic and functional pharmacological studies. J Auton Nerv Syst 1995;53: 115–125.

68 Paciga M, Vollmer C, Nurse C. Role of ET-1 in hypoxia-induced mitosis of cultured rat carotid body chemoreceptors. Neuroreport 1999;10:3739–3744.

69 Galperin MY, Rigden DJ, Fernandez-Suarez XM. The 2015 Nucleic Acids Research Database Issue and molecular biology database collection. Nucleic Acids Res 2015;43: D1–5.

70 Cunningham F, Amode MR, Barrell D et al. Ensembl 2015. Nucleic Acids Res 2015; 43:D662–669.

71 Leek JT, Johnson WE, Parker HS et al. The sva package for removing batch effects and other unwanted variation in high-throughput experiments. Bioinformatics 2012;28:882–883.

See www.StemCells.com for supporting information available online.